THz Photoconductive Devices: Photoconductive Switches and Photomixers

Researchers in the THz field struggled mightily during the 1960s through the 1980s to develop fundamental coherent sources. Among the many devices explored were IMPATT diodes, resonant tunneling diodes, Josephson-junction oscillator (arrays), and superlattice Block oscillators. Amongst the laser devices were cyclotron resonance (Landau level) intersubband lasers, coupled-quantum-well intersubband lasers, and spin-flip Raman lasers. All of these proved very difficult, even at cryogenic temperatures, so never gained widespread use, let alone commercial viability.

Then in the late 1980s and early 1990s a big breakthrough occurred with the advent of subpicosecond-lifetime (aka "ultrafast") photoconductors, as summarized quickly in Notes#5. These offered a means of generating useful levels of THz power using all room-temperature components, and took advantage of parallel developments in photonics technology. The first breakthrough was the photoconductive (i.e., "Auston") switch. The Auston switch cleverly utilized mode-locked laser technology. The second breakthrough was the photoconductive mixer (or "photomixer" for short) that took advantage of single-frequency, tunable solid-state (e.g., Ti:sapphire) and semiconductor (e.g., GaAs/AlGaAs heterojunction DBR) lasers.

Before discussing these devices in detail, we will first address two important effects in all photoconductors: square-law absorption and the Shockley-Ramo effect. The photoconductor in both the Auston switch and photomixer occur in bulk form; that is, they are a homogeneous material with two metal contacts. As in any semiconductor device, the coupling to the external circuit is a critical issue. On first glance, one might expect the coupling of photogenerated electrons and holes to the external circuit to be delayed by their respective transit times to the contacts – clearly a significant delay for any THz device. But this turns out to not be the case. In fact, the external circuit begins to respond to the effect of the photogenerated electron-hole pair immediately after the dc bias field begins to separate the two carrier types through the effect of carrier *drift*. This coupling to the external circuit was explained first in an elegant theorem due two separate papers in the late 1930s – one by Shockley and one by S. Ramo (the same Ramo comprising the "R" of TRW).

Internal Photoelectric Effect in Semiconductors

From fundamental semiconductor physics we know that the generation of electron-hole pairs by cross-gap photon absorption can be described semi-classically with the carrier wave functions expressed as quantum-mechanical (e.g. Bloch) wave functions and the electromagnetic energy expressed through the classical Poynting vector or, equivalently, the intensity. What results (from Fermi's golden rule) is an expression for the photocarrier generation rate g(t)

$$g(\vec{r},t) = \frac{\alpha I(\vec{r},t)}{h\nu} = \frac{\alpha E^2(t)}{Z_0 h\nu} \qquad [\mathrm{m^{-3}\text{–}s^{-1}}] \qquad (1)$$

where α is the absorption coefficient, E is the time-dependent optical electric field measured in the medium at the point $\vec{r}$ where absorption occurs, Z_0 is the intrinsic impedance of the medium, and hv is the optical photon energy. In going from I to E, the electric field is being treated classically, so (1) is generally regarded as "semiclassical".

The first equality in (1) is sometimes called the photoelectric law, first deduced by Einstein and the primary citation for his Nobel Prize in 1921. It is interesting that all of the early work on the photoelectric effect pertained to the creation of photoelectrons at air-solid interfaces, otherwise known as photocathodes. Later this effect was discovered to occur within solids and was called the "internal photoelectric effect." When it occurred in materials such as semiconductors having good electron transport properties (i.e., high mobility), significant changes in the electrical conductivity were found to occur. This led to the description "photoconductivity."

The second equality is critical for THz ultrafast photoconductive devices because of the *quadratic* dependence on electric field. This is what makes the ultrafast photoconductors "self-rectifying." So in response to a mode-locked laser, the photocarrier density can be computed in terms of the "envelope" of the optical pulse rather than the instantaneous electric field. And in response to two frequency-offset cw lasers, the photocarrier density shows a time-varying term at the difference frequency – the same effect as occurs in microwave mixers in which the current has a *quadratic* dependence on voltage.

Shockley-Ramo Effect and Current Impulse Response Function

Suppose one has a parallel-plate capacitor in which the internal electric field is uniform and the plates are separated by distance D. If an electron or hole is suddenly created somewhere inside the capacitor, it will initially have zero velocity but immediately be accelerated by the electrostatic force eE. In the process, its velocity v(t) will increase rapidly as will the kinetic energy. The interesting question addressed independently by Shockley and Ramo is what effect this acceleration process has on the current i(t) in the external circuit connected to the capacitor. They showed that the effect is immediate and can be expressed in simplest form as $i(t) = ev(t)/D$. If a carrier traverses the entire thickness of the capacitor and the velocity is constant or nearly constant during the entire process (not a bad assumption if the velocity quickly saturates, as it tends to do in semiconductors), then $i(t) = ev/D = e/T$ where T is the transit time between the plates.

In Notes#6 we derived the electron-hole pair concentration $\rho(t)$ in response to a short pulse in photon power that generates electron-hole pairs. If this generation occurs in the parallel-plate capacitor under high bias field and starts at time t = 0 (for simplicity), then $\rho(t)$ must be combined with the Shockley-Ramo effect to get the external-circuit electrical-current *response*. The response function of greatest use for circuits and systems calculations is the current impulse response, h(t) which is related to the photocarrier impulse response $\rho_i(t)$ by

$$h(t)= [(e/T)\rho_i(t)]\theta(t) \qquad (2)$$

where $\theta(t)$ is the unit step function, needed to satisfy "causality" (i.e. that the response not occur before the laser pulse), and $\rho i(t)$ is the response to a single electron-hole pair.

The quantity ρi(t) can indeed be derived from the more general result ρ(t) under special conditions. In Notes#6 we found for a Gaussian laser pulse,

$$\rho(t) = \frac{\alpha_0 B P_{o,pump}}{h\nu}\exp(-t/\tau)\left\{\frac{\sqrt{\pi}\cdot\exp[1/(4b\tau^2)]}{2\sqrt{b}}\left[erf(\sqrt{b}\cdot t - \frac{1}{2\sqrt{b}\cdot\tau}) + 1\right]\right\} \tag{3}$$

But as alluded to graphically in HW#4, this expression becomes relatively simple in the "impulse limit" when the rise- and fall-times of the laser pulse become much less than the recombination time: i.e., $(b)^{1/2}\tau >> 1$. In this case the erf function very rapidly approaches unity, and the concentration approaches the simple form $\rho_i(t) = A\exp(-t/\tau)$ where A is a complicated function of many parameters, but the time dependence is just the decaying exponential. This allows us to write

$$h(t)= [(e/T)\exp(-t/\tau)]\theta(t) \tag{4}$$

Given this expression, the electrical current is found by convolution using one of the most powerful techniques in all of electrical engineering – linear response theory. Accordingly, the output current is the convolution between the impulse response and the generation function

$$i(t) \equiv \int_{-\infty}^{t} h(t-t')G(t')dt' = \int_{0}^{t}\frac{e}{T}\exp[-(t-t')/\tau]G(t')dt' \tag{5}$$

where G is the net generation rate over the entire volume of the capacitor. The utility of this expression is in distinguishing ultrafast photoconductive devices based on the difference in their respective G(t) terms. This has the virtue of producing calculations of their THz output power with minimal complexity.

Please note that the above approach is intentionally simplified to emphasize the dynamic and engineering principles behind ultrafast photoconductive devices. In reality, both electrons and holes must be separately accounted for, the generation rate is dependent on position in the capacitor, and the velocity is not a constant in time. In fact, ultrafast devices are not even parallel plate capacitors ! Instead they tend to be planar-type capacitors to simplify optical coupling and facilitate direct integration in planar transmission lines, as described further below.

Auston Switch

In its simplest form the Auston switch is simply a gap in a uniform transmission line defined by thin-film metal fabrication on the top surface of an ultrafast photoconductor, as shown in Fig. 1(a). The transmission line shown is the coupled-strip line discussed earlier in the quarter in the lecture on quasi-TEM structures. The coupled-strip line is terminated in a planar antenna, shown as a planar strip dipole. The entire transmission line structure is biased with a voltage V_B through a (choke) inductor. The principal of operation is as follows. The gap in the transmission line initially creates an open-circuit condition. When a short pulse from a mode-locked laser arrives in the gap, a

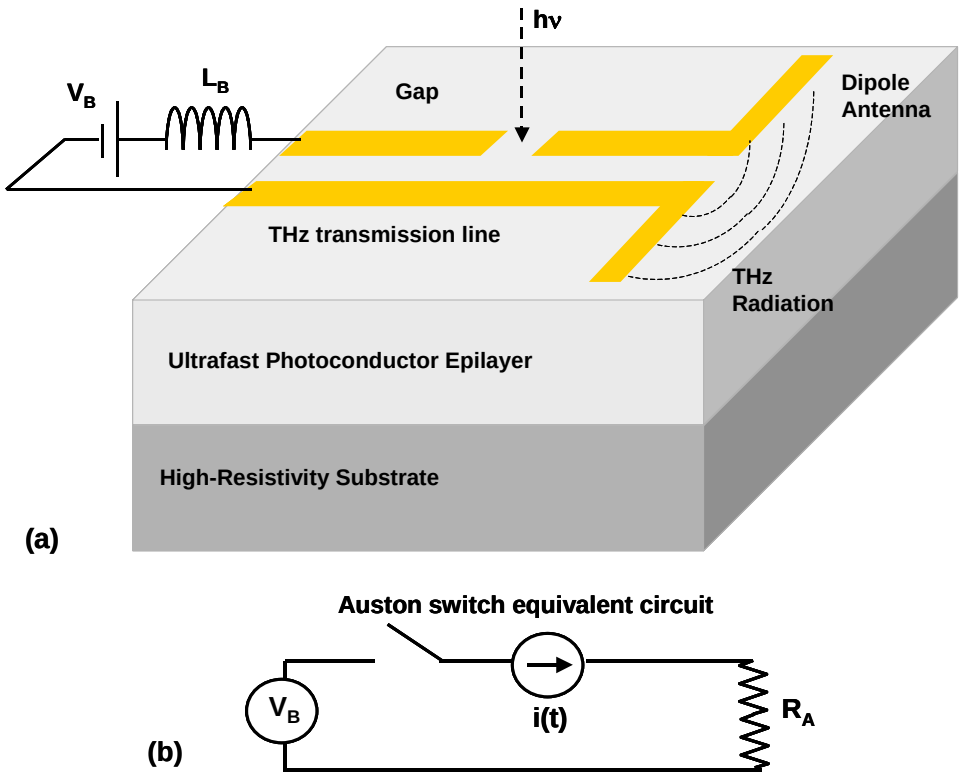

Fig. 1. (a) Perspective view of Auston switch. (b) Equivalent circuit.

shower of electron-hole pairs are generated in the first micron or two below the surface. The instantaneous concentration of these pairs is high enough to "short-out" the gap. When the laser pulse is terminated, the electron-hole pairs quickly recombine, creating an electrical impulse (or surge current) on the same time scale as the laser pulse. Because of the wide bandwidth of the planar transmission line, the electrical impulse propagates down the line to the antenna with minimal dispersion or droop. So upon reaching the antenna, the electrical pulse generates a significant amount of THz radiation that propagates primarily into the substrate.

To predict the temporal and spectral behavior of the Auston switch, we apply the linear response formalism developed above with a generation function G(t) consistent with the electrical current impulse response; i.e., a much shorter laser pulse than τ. The simplest form for G(t) is then the Dirac delta function

$$G(t) \approx \frac{U_{abs}}{h\nu}\delta(t) \tag{6}$$

where U_{abs} is the single pulse energy absorbed within the active volume of the switch. In addition, the external current must be consistent with the laser pulse stream. Ultrafast mode-locked lasers are characterized by a pulse-to-pulse separation time t_{rep} (corresponding to pulse repetition rate $f_{rep} = 1/t_{rep}$) that is necessarily much greater than the single pulse rise- and fall times. And the high pulse energy is possible because each pulse is uncorrelated from the others. In other words, i(t) for a single pulse must be

truncated to be physically admissible. Truncating between 0 and t_P, we get a current response

$$i(t) = \theta(t)\theta(t + t_{rep}) \int_0^t \frac{e}{T} \exp[-(t - t')/\tau] G(t') dt' = \theta(t)\theta(t + t_{rep}) \frac{U_{abs}}{h\nu} \frac{e}{T} \exp[-t/\tau] \quad (7)$$

To be electrically admissible, it is important to incorporate the switch into a THz equivalent circuit, perhaps the simplest being that shown in Fig. 1(b). The gap is modeled like a transient switch, and the antenna like an ideal load of static resistance R_A matched to the transmission characteristic impedance Z_0. The voltage generated across the antenna is then approximately $i(t)R_A$ but subject to the constraint implied by 1(b) that *the antenna voltage can not exceed the bias voltage* V_B :

$$\mathbf{v(t) = \theta(v + V_B) R_A \theta(t)\theta(t + t_{rep}) \frac{U_{abs}}{h\nu} \frac{e}{T} \exp[-t/\tau] \le V_B \theta(t)\theta(t + t_{rep}) \exp(-t/\tau)} \quad (8)$$

To estimate the power radiated, we first take the Fourier transform of the voltage response

$$\mathbf{u(\omega) = \frac{1}{\sqrt{2\pi}} \int_{-\infty}^{\infty} v(t) \exp(j\omega t) dt \le \frac{1}{\sqrt{2\pi}} \int_0^{t_{rep}} V_B \exp(-t/\tau) \exp(j\omega t) dt} \quad (9)$$

$$= \frac{V_B \tau}{\sqrt{2\pi}} \frac{1 - \exp(-t_{rep}/\tau) \exp(j\omega t_{rep})}{1 - j\omega\tau}$$

From integral transform theory, the single-pulse energy spectrum $S_E(\omega)$ is just $u(\omega)u^*(\omega)/R_A$,

$$S_E(\omega) \equiv u(\omega)u^*(\omega)/R_A = \frac{(V_B\tau)^2}{2\pi R_A} \cdot \frac{1 + \exp(-2t_{rep}/\tau) - 2\exp(-t_{rep}/\tau)\cos\omega t_{rep}}{1 + \omega^2\tau^2} \quad (10)$$

And as in communications and radar theory where pulse streams are routine, the power spectrum $S(\omega)$ is found by averaging over m successive pulses,

$$S\ (\omega) \equiv \frac{m \cdot S_E(w)}{m \cdot t_{rep}} = \frac{(V_B\tau)^2}{2\pi R_A t_{rep}} \cdot \frac{1 + \exp(-2t_{rep}/\tau) - 2\exp(-t_{rep}/\tau)\cos(\omega \cdot t_{rep})}{1 + \omega^2\tau^2} \quad (11)$$

To check this power spectrum for physical correctness, we need only evaluate it at $\omega = 0$ (dc case). For this purpose, we can temporarily assume $t_{rep} << \tau$, corresponding to a steady-state with practically no change in v(t). Second order expansion of the exponentials in the denominator then yields,

$$S\ (\omega = 0) = \frac{(V_B\tau)^2}{2\pi R_A t_{rep}} \cdot \left(\frac{t_{rep}}{\tau}\right)^2 = \frac{V_B^2}{2\pi R_A} t_{rep} = \frac{V_B^2}{R_A \omega_{rep}} \quad (12)$$

the expected spectral density for the dc term across a resistor.

A more practical and interesting form results from plotting S(ω) under the typical ultrafast conditions $t_{rep} >> \tau$. In this case the two exponential terms in the numerator are negligible, and one gets the useful expression

$$S\ (\omega) \approx \frac{(V_B \tau)^2}{2\pi \cdot R_A t_{rep}} \cdot \frac{1}{1+\omega^2\tau^2} \tag{13}$$

This is the classic Lorentzian spectrum so pervasive in nature and a hallmark of photoconductive response. The power spectrum is down a factor of two (i.e., -3 dB) at $\omega\tau = 1$, corresponding to a bandwidth of $f_{3\text{-dB}} = (2\pi\tau)^{-1}$. Integrating the spectrum over all frequencies yields the total delivered power

$$P_L \approx \int_{-\infty}^{\infty} \frac{(V_B \tau)^2}{2\pi \cdot R_A t_{rep}} \cdot \frac{d\omega}{1+\omega^2\tau^2} = \frac{(V_B \tau)^2}{2\pi \cdot R_A t_{rep}} \frac{1}{\tau} \tan^{-1}(\omega\tau)\,|_{-\infty}^{\infty} = \frac{(V_B)^2 \tau}{2 \cdot R_A t_{rep}} \tag{14}$$

Note that the ratio τ/t_{rep} is just the duty cycle, so the load power can be considered as the average ac power times the duty cycle.

As an example we consider an ultrafast GaAs Auston switch being driven by a Ti:sapphire mode-locked laser. For the ultrafast GaAs we assume τ = 200 fs, and for the laser t_{rep} = 10 ns. The Auston switch is assumed to have a 10-micron-wide gap and is biased with V_B = 50 V. The antenna is assumed to have a radiation resistance of R_A = 100 Ω- typical of planar antennas radiating into a GaAs substrate. This results in a total power $P_L = 2.5\text{x}10^{-4}$ W = 0.25 mW – an impressive power by THz standards. But this is distributed over the entire spectrum, primarily out to $f_{3\text{-dB}}$ = 796 GHz. Of more importance to "coherent" applications such as spectroscopy, radar, and communications is the power spectral density at some interesting frequency, such as 600 GHz. Substitution of these parameters into the spectral density then yields

$$S\ (\omega)\,|_{f=600GHz} \approx \frac{(V_B \tau)^2}{2\pi \cdot R_A t_{rep}} \cdot \frac{1}{1+\omega^2\tau^2} \approx 1\text{x}10^{-17}\ \text{W/Hz} \tag{15}$$

So in a typical "band-limited" system or experiment with $\Delta\omega$ = 100 MHz, the average power available from the Auston switch will be ~ 1 nW. And this is an upper-limit result based on the assumption that the full V_B can be impressed on the antenna instantaneously. In reality, if the gap is made large enough (~10 μm diam or more) to easily accommodate a focused laser beam, the Shockley-Ramo effect will prevent from the "switch" from being fully closed at the peak-power point, and the output power will be substantially less.

In concluding the Auston switch analysis, note that the derived power spectrum appears to be continuous and monotonic, defying common sense for such a pulsed-mode device. This is a consequence of our simplified analysis in which we evaluated the power spectrum of only one "truncated" laser pulse and added the individual expression to get the overall output power spectrum. For greater accuracy, the power spectrum should be calculated for the entire mode-locked laser pulse train expressible as the following infinite series,

$$P_T(t) = \sum_n P_1(t - n \cdot t_{rep}) \tag{16}$$

where P_1 is the power form for an individual pulse and n is any integer from $-\infty$ to ∞. As in standard digital communication or radar analyses, this "comb"-like pulse train leads, after Fourier transformation, to a conjugate "comb" in the frequency domain. Each "tooth" of the comb is located at $m/t_{rep} = m\, f_{rep}$. So the more accurate power spectrum is actually discrete. The continuous one derived here is an average through the discreteness, so is actually a rather accurate representation of what would be measured in the THz domain by a time-averaging power meter, a thermal detector (e.g., Golay cell or bolometer), or a square-law rectifier followed by an integration circuit having an integration time >> t_{rep}.

Photomixers

The majority of THz photomixers demonstrated to date have been fabricated from interdigital electrode structures, as shown in Fig. 2(a). The gap between neighboring electrodes is made much larger than the electrode width so that a majority of light incident from the top side enters the photoconductive material, as shown in Fig. 2(b). Strong photomixing can occur if the incident light consists of two frequency-offset lasers, such as GaAs/AlGaAs laser diodes. Then the quadratic nature of the cross-gap absorption with respect to the electric field, discussed earlier, mixes the fields and creates an ac photocurrent between the electrodes oscillating at the difference frequency between the lasers.

The ac photocurrent is usually transformed into THz power by coupling the electrodes to a low-loss antenna, such as the resonant dipole shown in Fig. 2(a). According to the principles discussed below, the THz output power is limited by the external quantum efficiency of the photomixer, the photocarrier recombination time, circuit-related (e.g., RC) rolloff of the photomixer circuit, and by deleterious heating effects that occur with high optical drive intensity. Note that the photomixer behaves in some ways like a field-effect transistor (FET), but with a photonic gate instead of the usual metal gate. So unlike an FET, the bandwidth of the photomixer is not limited by the gating effect because *optical coupling requires no metal electrode and, therefore, adds no capacitance.*

When designed for THz operation, a photomixer usually has an electrode width of ~0.2 μm, a gap width of ~1.5 μm, and total active area of ≈100 μm^2. If the gaps are made much smaller to achieve high photoconductive gain, the capacitance gets large and limits the power and O-E efficiency at sub-THz frequencies through RC rolloff, where R is antenna radiation resistance. If the gaps are made much larger to reduce the capacitance, the inverse transit time and associated photoconductive gain G_P decay, limiting the output power and O-E efficiency at moderate drive power levels. If the area is made much larger to allow for more optical pump power, the capacitance increases and causes RC roll off well below 1 THz. If the area is made much smaller, burnout invariably occurs because of the high junction temperature that results from the combination of optical drive and electrical bias.

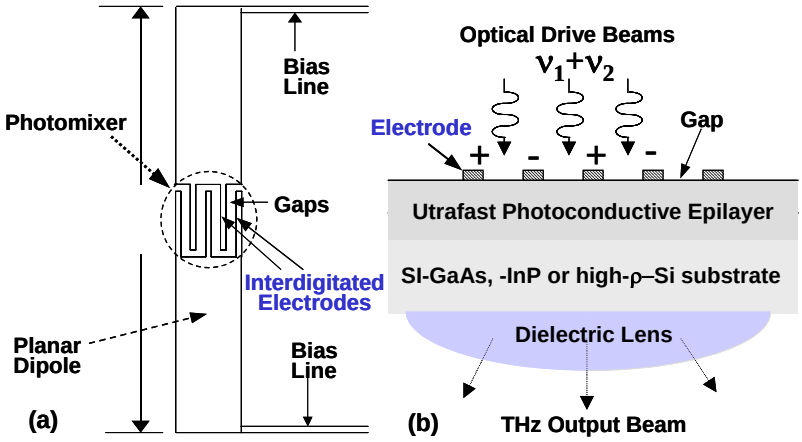

Fig. 2. (a) Top view of interdigitated-electrode vertically-driven photomixer coupled to a planar dipole antenna (b) Cross-sectional view of photomixer showing bottom-side coupling of THz radiation through a dielectric lens (not to scale) to free space.

Besides its small area and low specific capacitance, another key benefit of the interdigitated-electrode photomixer is that it naturally creates a *balanced* current feed for simple planar antennas such as dipoles, slots and a class of self-complementary spirals. No balun or similar circuit is required. The spirals are particularly useful because of their inherently wide instantaneous bandwidth (~1 decade or more). If judiciously aligned with the operating band of the photomixer, the spiral antenna will combine with the photomixer to create a THz free-space source with exceptionally high tuning bandwidth – a THz sweep oscillator. Such a source has never existed in the THz region and, as in lower frequency bands, could be a strong enabler for scientific and technological purposes.

To predict the THz performance of the photomixer, we start by deriving the time-dependent photogeneration g(t). The period of the optical electric field that can excite cross-gap carriers in GaAs is to small to be detected by electrical means. But when the electric field consists, by linear superposition, of two independent sinusoidal optical fields, E_1 and E_2 at different frequencies, the photogeneration becomes

$$g(\vec{r},t)=\frac{\alpha[E_1(t)+E_2(t)]^2}{Z_0 h\nu}=\frac{\alpha[E_1\cos\omega_1 t+E_2\cos(\omega_2 t+\phi)]^2}{Z_0 h\nu} \qquad (17)$$

$$\approx\frac{\alpha}{Z_0 h\nu}\left[E_1^2/2+E_2^2/2+E_1E_2\cos(\Delta\omega t-\phi)\right]=\frac{\alpha}{h\nu}\left[I_1+I_2+2\sqrt{I_1I_2}\cos(\Delta\omega_1 t-\phi)\right]$$

where ϕ is the phase difference between the two field, $\Delta\omega = \omega_1 - \omega_2$, and I_1 and I_2 are the time-averaged intensities of each field at the point of absorption. The third term is the beat-note or difference-frequency term, which can comprise a significant fraction of g_e if I_1 and I_2 are comparable. . Clearly α is an important parameter. For example in GaAs at $\lambda = 0.78$ μm, $\alpha \approx 10^4$ cm^{-1}.

For the purpose of calculating the THz output spectrum and contrasting with Auston switches, it is simplest to average over the active volume of the photomixer in a

process that yields a (quantum) efficiency factor η that is a combination of power coupling and mixing efficiencies. The resulting net photomixing generation rate is

$$G(t) = \frac{\eta}{h\nu}\left[P_1 + P_2 + 2\sqrt{P_1 P_2}\cos(\Delta\omega_1 t - \phi)\right] \tag{18}$$

Given a total optical power $P_T = P_1 + P_2$, it is simple to prove that the division between P_1 and P_2 that maximizes the contribution to G is simply $P_1 = P_2$.

Given this generation function and the photoconductive current impulse response derived earlier, one can derive the external current response

$$i(t) \equiv \int_{-\infty}^{t} h(t-t')G(t')dt' = \int_{-\infty}^{t} \frac{e}{T}\exp[-(t-t')/\tau]G(t')dt' \tag{19}$$

We can simplify the analysis somewhat by re-writing G(t) in phasor form $G(t) \equiv G_0 + \mathrm{Re}\{\widetilde{G}\, e^{j\Delta\omega t}\}$ so that $G_0 = (\eta/h\nu)(P_1+P_2)$ and $\widetilde{G}$, a complex constant, is given by $(\eta/h\nu)2(P_1P_2)^{1/2}e^{-j\phi}$. Straightforward integration of (19) then leads to the photomixing short-circuit current

$$i(t) = eG_0\left(\frac{\tau}{T}\right) + e\frac{\tau}{T}\mathrm{Re}\left\{\frac{\widetilde{G}e^{j\Delta\omega t}}{1 - j\Delta\omega\cdot\tau}\right\} \tag{20}$$

Completion of the Re{} operator in leads to the physically measurable result

$$i(t) = eG_0\left(\frac{\tau}{T}\right) + e\,|\widetilde{G}|\left\{\frac{\tau}{T}\frac{\cos(\Delta\omega t - \phi) - \Delta\omega\tau\ \ \sin(\Delta\omega t - \phi)}{1 + (\Delta\omega\tau\ )^2}\right\} \tag{21}$$

Inspection of the limiting behavior as $\Delta\omega \to 0$ indicates that both the dc and ac terms are multiplied by the factor τ/T. In principle, this factor can be significantly greater than unity, and thus is traditionally called the *photoconductive gain* G_P. Physically if $G_P > 1$, then *more than one* photocarrier can be delivered to the external circuit for each photon absorbed by the detector. *This is not a violation of the laws of thermodynamics*. Any difference between the power delivered to the load resistor and the incident optical power is provided by the required bias supply. This is an important distinction between ohmic MSMs and PiN photodiodes (or Schottky MSM detectors), which do not require external bias. On the other hand, PiN photodiodes and Schottky MSM detectors cannot provide a photoconductive gain greater than unity under any condition.

From the THz generation standpoint, the most important aspect of Eqn (20) is the time-varying term which can be written in phasor form as $i(t)=\mathrm{Re}\{\widetilde{i}\ e^{j\Delta\omega t}\}$, where

$$\widetilde{i}\,(\Delta\omega) = \frac{2e}{h\nu}\left((P_{1,0}\cdot P_{2,0})^{1/2}e^{-j\phi}\,\frac{\eta}{1 - j\Delta\omega\cdot\tau}\right) \tag{22}$$

From fundamental circuit theory, the magnitude can be considered as the maximum short-circuit current that the photomixer can deliver to any load ,

$$i_s = \sqrt{\widetilde{i}\cdot\widetilde{i}^{\,*}} = \frac{2e}{h\nu}\left((P_{1,0}\cdot P_{2,0})^{1/2}\left[\frac{\eta^2}{1 + (\Delta\omega\cdot\tau)^2}\right]^{1/2}\right) \tag{23}$$

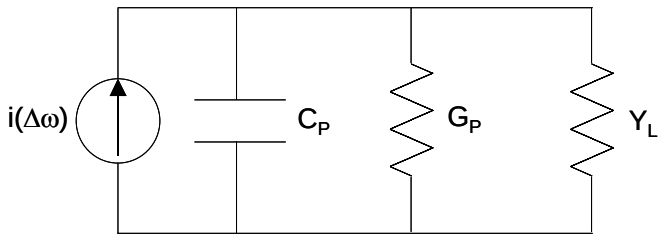

Fig. 3. Equivalent circuit of interdigitated-electrode photomixer.

If we maximize this with respect to the total optical power P_0 , we find $P_{1,0} = P_{2,0} = P_{in}/2$, and

$$i_s = \frac{\eta e P_{in}}{h\nu}\left[\frac{1}{1+(\Delta\omega\cdot\tau)^2}\right]^{1/2} \equiv S P_{in}\left[\frac{1}{1+(\Delta\omega\cdot\tau)^2}\right]^{1/2} \tag{24}$$

From this we see that the magnitude of ac photomixer current at $\Delta\omega = 0$ is *exactly* equal to the dc photocurrent. So the dc responsivity is a good indicator of the THz photomixer performance. For example, given the parameters $\eta = 0.05$ and $h\nu = 1.59$ eV, we find $S = 0.03$ A/W – close to the experimental value for good photomixers.

To complete the analysis of photomixers at a level useful for engineering design purposes, circuit effects must be included. The short-circuit current of Eqn (24) represents only the *conduction* current that flows between the electrodes in the presence of photogeneration and a dc bias field. From Maxwell's generalization of Ampere's law we also know that a displacement current $\varepsilon dD/dt$ must flow between the electrodes. From a circuit standpoint, this displacement current can be represented by the capacitance C_P calculated for the electrodes in Fig. 2. This capacitance is almost always significant in photomixers at THz frequencies and leads to the equivalent-circuit shown in Fig. 3. In this circuit G_P is the differential resistance of the photomixer at the bias point, given approximately by $I_0/V_b = SP_{in}/V_b$. As in the lower RF bands, most THz load circuits can be represented as a complex admittance $Y_L = G_L + jB_L$, at least over limited bandwidths. But only the real part of Y_L is capable of sinking the power corresponding to the difference-frequency generation term.

Given this circuit we can calculate the current phasor in the load by simple current divider action between G_P, C_P, and Y_L :

$$\tilde{i}_L \approx \frac{\tilde{i}(\omega)}{1+j\omega R_L C} = \frac{2e}{h\nu}(P_{1,0}\cdot P_{2,0})^{1/2} e^{-j\phi}\left[\frac{\eta}{1-j\Delta\omega\cdot\tau}\right]\left[\frac{G_L}{(G_L+G_P)+j(\omega C_D + B_L)}\right] \tag{25}$$

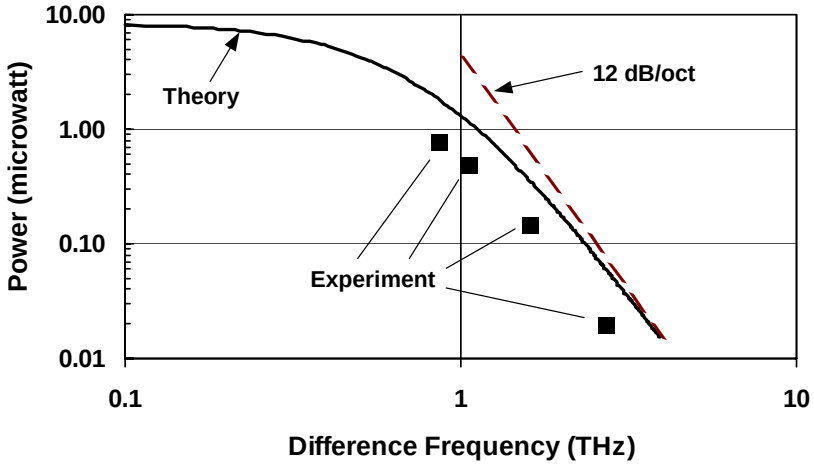

Fig. 4. Experimental results for a broadband LTG-GaAs photomixer at room temperature Also shown is the theoretical curve from our analysis and the parameters of the given photomixer.

and the power in the load is

$$P_L = \frac{|\tilde{i}_L|^2}{2G_L} \approx 2\left(\frac{e}{h\nu}\right)^2 \mathrm{P}_{1,0}\cdot\mathrm{P}_{2,0}\left|\frac{\eta}{1-j\Delta\omega\cdot\tau}\right|^2 \frac{G_L}{(G_L+G_P)^2+(\omega C_D+B_L)^2} \qquad (26)$$

This expression shows that the circuit introduces additional frequency dependence to the load power through the reactive part (i.e., B_L) of the load circuit. For the optimum case of $P_{1,0} = P_{2,0} = P_{in}/2$, we find

$$P_L = \frac{1}{2}|\tilde{i}_L|^2\ R_L = \frac{1}{2}\mathrm{S}^2\mathrm{P}_{in}^2\cdot\frac{1}{1+(\Delta\omega\cdot\tau)^2}\cdot\frac{G_L}{(G_L+G_P)^2+(\omega C_D+B_L)^2} \qquad (27)$$

This expression is very useful for estimating the output of THz photomixers. It can be analyzed in two general cases: (1) broadband loads for which $B_L \approx 0$, and (2) resonant loads for which $\omega C_D \approx B_L$ at the resonant frequency. It can also be used for performance optimization.

The simplest THz loads to design and fabricate are the broadband self-complementary antennas, such as logarithmic and square spirals. Submicron resolution is not required on any features except the interdigitated electrodes. The antenna pattern is guaranteed to be rather symmetrical about the optical axis of the photomixer, and dc biasing is rather trivial. One need only wrap the spiral with enough turns so that the lowest frequency of interest radiates away before reaching the outer extent of the spiral. Then, to dc bias the device one need only bond wire to the outer extent. No chokes or other RF passives components are required. Under these conditions, the antenna impedance is given approximately by the reactance-free expression, $R_A \approx 60\pi/(\varepsilon_{eff})^{1/2} = 72\ \Omega$ for $\varepsilon_{eff} = (1+\varepsilon_r)/2 = 6.9$ for $\varepsilon_r = 12.8$ of GaAs.

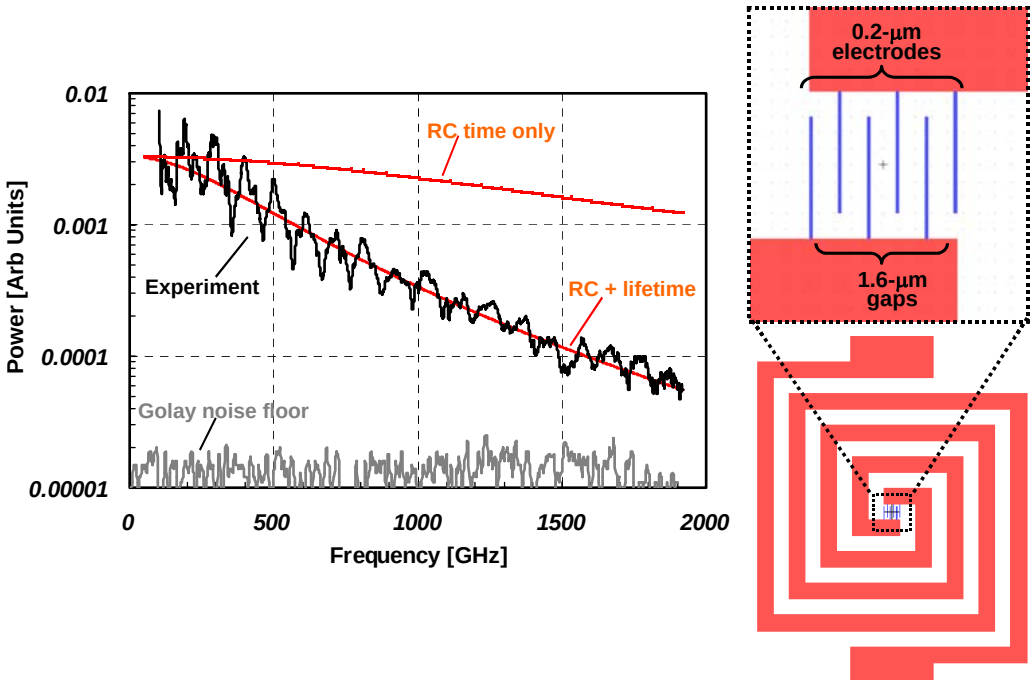

Fig. 5. (Left side) Experimental power spectrum from ErAs:GaAs photomixer along with noise floor and theoretical modeling curves. (Right side) Interdigitated-electrode structure located at the driving point of a two-turn, self-complementary square spiral antenna. The absolute power at 1 THz corresponds to ≈1 μW.

Shown in Fig. 4 is the best reported THz output power from an *LTG*-GaAs photomixer coupled to a broadband antenna - a two-turn log spiral antenna. The interdigitated structure has eight 0.2-micron-wide electrodes, seven 0.9-micron gaps. The LTG-GaAs had a measured, small-bias lifetime of 0.25 ps. The structure was fabricated at the driving point of a two-turn logarithmic spiral antenna. The measured power output is just above 1 μW up to about 1 THz and then falls rapidly at higher frequencies. Superimposed on this plot is the theoretical maximum broadband power for the following parameters: C = 2.1 fF, G_L = 0.014 S, B_L = 0, P_{in} = 78 mW, $v_e = v_h$ = 0.6×10^7 cm/s, and S = 10 mA/W. The agreement between experiment and theory in terms of frequency roll-off is remarkably good, both curves approaching 12 dB/octave at frequencies for which $\omega\tau > 1$ and $\omega C/G_L > 1$. The discrepancy in absolute power is about a factor of two – also very good considering the number of factors that can reduce the power coupled from the photomixer to the THz bolometer in the experiments.

More recently, the Brown + Gossard groups at UCSB have improved the broadband photomixer performance by using ErAs:GaAs and coupling it to a two-turn self-complementary square spiral. The experimental results and top-view of the photomixer design are shown in Fig. 5. The absolute power in the power spectrum corresponds to approximately 1 μW at 1 THz. Also shown is a fit to the experimental curve using the formalism developed here with the THz output written in the form

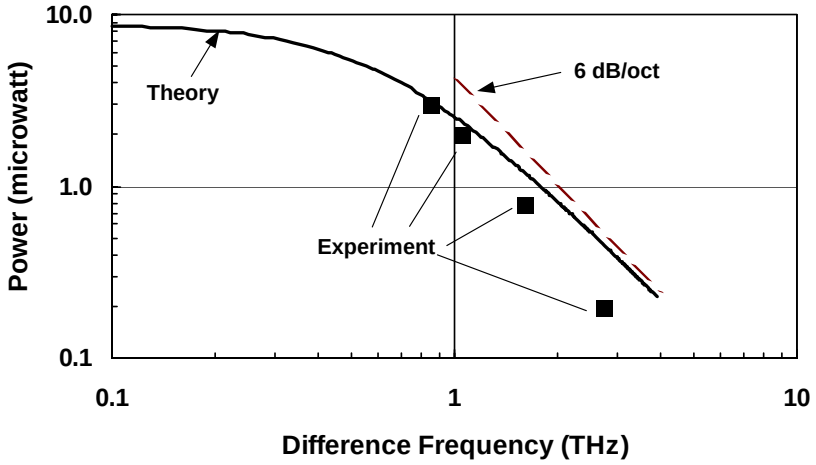

Fig. 6. THz output power from resonant (dual slot) antenna

$$P(\omega) = P_0 \left[1+(\omega\tau_{RC})^2\right]^{-1} \left[1+(\omega\tau_{eh})^2\right]^{-1} \tag{28}$$

where P_0 is the low-frequency output and ω is the circular difference frequency. The capacitance of the six-finger structure in Fig. 5 is estimated from electrostatics to be approximately 1.5 fF,[1] leading to $R_aC_e \approx 0.11$ ps. The corresponding RC-limited power spectrum is plotted in Fig. 5 assuming $P_0 = 0.0033$.

Resonant load antennas are not as simple to design or implement as broadband antennas because of difficulties in simulation and design. By definition, resonant antennas have a significant conductance and susceptance that depend strongly on frequency and on the geometry of the antenna. And resonant antennas do not generally provide a symmetric beam or a simple means of dc biasing of the device.

The first reported resonant antennas coupled to photomixers were full-wave dipoles and slots[2] In comparison to log spiral antennas, both displayed a resonant THz output power having a peak consistent with the resonant frequency for the given antenna type. However, with a slot or dipole it is always questionable whether all the power is being collected as both types have distinctly asymmetric antenna patterns in the E and H planes.

To improve the radiation pattern and provide even better cancellation of the electrode capacitance, the group at Lincoln Lab also fabricated an LTG-GaAs photomixer in a sequence of twin slot antennas after successful demonstration of this approach in SIS mixers. The structure consisted of two 100-micron slots separated by __ micron with the interdigitated structure located at the mid-way point. The interdigitated structure had four 0.2-micron-wide electrodes and three 1.8-micron gaps. The LTG-GaAs had a measured, small-bias lifetime of 0.25 ps. The measured output power is plotted in Fig. 6: 3.0 μW at 850 GHz, 2.0 μW at 1050 GHz, 0.8 μW at 1600 GHz, and 0.2 μW at 2700 GHz. Superimposed on this plot is the theoretical maximum resonant power

[1] J.B.D. Soole and H. Schumacher, IEEE Trans. Electron Dev., **37**, p. 2285 (1990).
[2] K.A. McIntosh, E.R. Brown, K.B. Nichols, O.B. McMahon, W.F. DiNatale, T.M. Lyszczarz, "Terahertz measurements of resonant planar antennas coupled to low-temperature-grown GaAs photomixers," Appl. Phys. Lett, vol. 69, p. 3632 (1996).

predicted by our analysis for the following parameters: C = 0.58 fF, G_L = 1/215 = 0.0046 S, B_L = 0.02, P_{in} = 56 mW, and S = ___ mA/W. The agreement between experiment and theory is even better than in the broadband case. The discrepancy in absolute power is less than 10% at 850 and 1050 GHz , but grows to 80% at 2700 THz.

Contrasts and Advantages of Ultrafast Photoconductive Devices

We have seen that the Auston switch is inherently a time-domain device and the photomixer is a frequency domain device. Interestingly, the Auston switch provides more average power. But the photomixer provides much higher THz spectral density.

Three technological breakthroughs have occurred during the past decade that make Auston switches and photomixers practical THz sources: (1) growth and fabrication of semiconducting material having photocarrier lifetime less than 1 ps, (2) modern microfabrication techniques that allow sub-micron electrode features to be patterned on the photoconductor surface, leading to sub-picosecond electrical time constants, and (3) integration of photomixer elements with compact planar antennas, leading to efficient coupling of the THz radiation to free space. A good example is the interdigitated-electrode photomixer coupled to a planar antenna, such as the dipole shown in Fig. 2.

An ancillary breakthrough that strongly supports the photomixer approach has occurred in the field of solid-state and semiconductor lasers. Solid-state materials such as Ti:Al_2O_3, have been developed that provide unprecedented values of gain-bandwidth so can provide very short pulses in mode-locked lasers, and high levels of power tunable over 10s of nm in cw lasers. Various techniques such as distributed Bragg reflectors, distributed feedback structures, and external cavities have all been integrated with semiconductor laser diodes to produce sources with useful output power (>1 mW) and high spectral purity. And in the popular fiber-optic telecommunication band around 1550 nm, the erbium-doped fiber amplifier (EDFA) has been developed that can boost the power of spectrally-pure laser-diode sources up to ~1-W level.

A key advantage of both ultrafast photoconductive devices over alternative THz-sources is bandwidth. The Auston switch is limited by the combination of mode-locked laser pulse width and photocarrier recombination time. The photomixer is limited by the combination of RC time constant and photocarrier lifetime. One might think that cw laser stability and tunability would pose a problem to photomixing, but the technology has come through. The reason is that relatively little tuning is required of the cross-gap pump lasers to produce THz difference-frequency tuning. Fig. 7 shows how little wavelength offset $\Delta\lambda$ is required to produce THz difference frequencies. The formula for this offset is simply $\Delta\nu = c|\Delta\lambda|/(\lambda_1\ \lambda_2)$, which is approximately given by $c|\Delta\lambda|/(\lambda)^2$ for $\lambda_1 \approx \lambda_2$. One curve assumes λ = 780 nm - probably the shortest-wavelength laser diode demonstrated to date. The other curve assumes λ = 1550 nm - probably the longest-wavelength laser diode to date. Note that at 780 nm and 1550 nm, a 1 THz difference occurs for a $\Delta\lambda$ of 2.05 nm and 8.05 nm, respectively. Both offsets are readily achieved with modern tunable laser-diode technology.

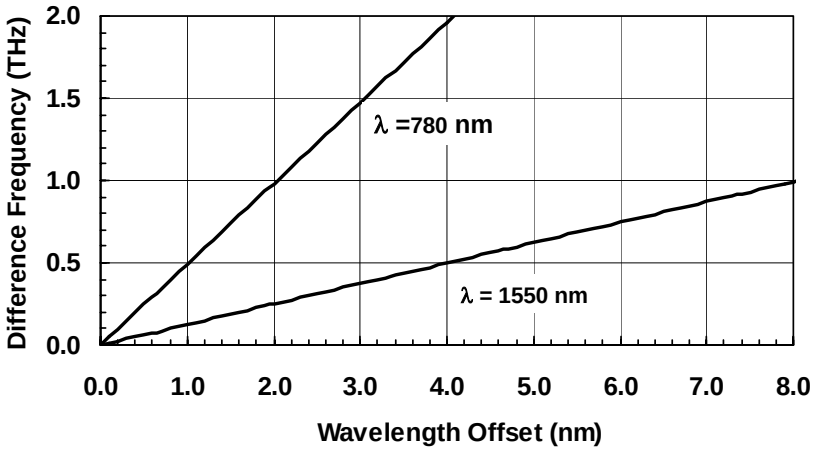

Fig. 7. Difference frequency as a function of wavelength offset for drive lasers at two popular wavelengths – 780 and 1550 nm.